A supermassive binary black hole with triple disks

Kimitake Hayasaki[1]

Yukawa Institute for Theoretical Physics, Kyoto University, Oiwake-cho, Kitashirakawa, Sakyo-ku, Kyoto 606-8502, Japan

kimitake@yukawa.kyoto-u.ac.jp

Shin Mineshige[1]

Yukawa Institute for Theoretical Physics, Kyoto University, Oiwake-cho, Kitashirakawa, Sakyo-ku, Kyoto 606-8502, Japan

and

Luis C.Ho[2]

The Observatories of the Carnegie Institution of Washington, 813 Santa Barbara Street, Pasadena, CA 91101, USA

ABSTRACT

Hierarchical structure formation inevitably leads to the formation of supermassive binary black holes (BBHs) with a sub-parsec separation in galactic nuclei. However, to date there has been no unambiguous detection of such systems. In an effort to search for potential observational signatures of supermassive BBHs, we performed high-resolution smoothed particle hydrodynamics (SPH) simulations of two black holes in a binary of moderate eccentricity surrounded by a circumbinary disk. Building on our previous work, which has shown that gas can periodically transfer from the circumbinary disk to the black holes when the binary is on an eccentric orbit, the current set of simulations focuses on the formation of the individual accretion disks, their evolution and mutual interaction, and the predicted radiative signature. The variation in mass transfer with orbital phase from the circumbinary disk induces periodic variations in the light curve of the two accretion disks at ultraviolet wavelengths, but not in the optical or near-infrared. Searches for this signal offer a promising method to detect supermassive BBHs.

Subject headings: black hole physics – accretion, accretion disks – binaries:general – galaxies:nuclei

1. Introduction

1.1. Scientific Motivation

Supermassive black holes are common in galactic nuclei and are considered to have coevolved with their host galaxies (Magorrian et al. 1998; Ferrarese & Merritt 2000; Gebhardt et al. 2000; Yu & Tremaine 2002; Di Matteo et al. 2005). Since galaxies grow through mergers, it is inevitable that supermassive binary black holes (BBHs) will form (Ebisuzaki et al. 1991). Supermassive BBHs evolves via three stages (Begelman et al. 1980; Yu 2002). First, each of the black holes sinks independently toward the center of the common gravitational potential due to dynamical friction with neighboring stars. When the separation between the two black holes becomes less than $\sim 1\,\mathrm{pc}$, angular momentum loss by dynamical friction slows down due to the loss-cone effect (Roos 1981; Makino 1997; Milosavljević & Merritt 2001). A hard binary forms during the second stage, whose orbit slowly shrinks, until the final stage where the black holes merge by emitting gravitational radiation. Recent hydrodynamic simulations of a gas-rich galaxy merger (Mayer et al. 2007) show that the interaction between the black holes and the surrounding stars and gas rapidly leads to the formation of a BBH. After the two black holes have reached the scale of the circumnuclear disk ($\sim 100\,\mathrm{pc}$), it takes less than 1 Myr for them to form a hard binary on scales of ~ 1 pc.

Despite the general expectation that BBHs should form naturally during the course of galaxy formation and evolution, the currently available observational evidence for BBHs have been largely circumstantial and indirect. These include the detection of X-shaped structures in radio galaxies (Merritt & Ekers 2002), double compact cores with a flat radio spectrum (Rodriguez et al. 2006), and close pairs of AGNs such as that seen in NGC 6240 (Komossa et al. 2003). As these systems evolve, we expect that their black holes would eventually form a strongly gravitationally bound binary on sub-parsec scales. Such small-scale binaries have been inferred to be present from the quasi-periodic outbursts detected in OJ 287 (Sillanpää et al. 1988) and the proper motions seen toward the compact radio core in 3C 66B (Sudou et al. 2003), but the interpretation of neither case is unambiguous.

In view of the astrophysical importance of BBHs, it would be desirable to devise robust methods for detecting them. Sundelius et al. (1997) showed that when two unequal-mass black holes interact, for instance in the aftermath of a minor galaxy merger, the impact of the secondary black hole on the accretion disk around the primary black hole may generate periodic flares. These authors invoked this model to explain the brightness variations in OJ 287. In supermassive BBHs with extreme mass ratios, the secondary black hole could be embedded in the accretion disk of the primary black hole and migrate toward it. The kind of disk-binary interaction offers a promising solution to the loss-cone problem (Ivanov et al.

1999; Gould & Rix 2000; Armitage & Natarajan 2002, 2005). Yu (2001) proposed that BBHs might be detectable from the integrated Fe Kα line of two accretion disks, which would give rise to an unusual profile with double or multiple peaks.

1.2. Our Previous Work

It is likely that a rotating gas disk (i.e., circumbinary disk) forms around supermassive BBH during the second stage of a gas-rich galaxy merger. If so, what will happen as a result of the interaction between the BBH and the circumbinary disk? Hayasaki et al. (2007), using a smoothed particle hydrodynamics (SPH) code (Benz et al. 1990; Benz 1990; Bate et al. 1995), investigated the accretion flow from a circumbinary disk onto the supermassive BBH on sub-parsec scales. In that study, the circumbinary disk was aligned with the binary orbital plane. They found that mass transfer can occur from the circumbinary disk to the supermassive BBH in two steps. First, the initially circularized circumbinary disk becomes elongated due to the azimuthal $m = 2$ component of the binary potential. The gas density then grows at the two points closest from the black holes. Next, when the gas reaches beyond the potential barrier of the binary, mass inflow is initiated by gas pressure so that the gas freely inspirals onto each of the black holes. This process repeats every binary orbit. The viscosity of the circumbinary disk is ineffective for the mass transfer process because the viscous timescale is much longer than the orbital period. For BBH systems on sub-parsec scales, the viscous timescale of the circumbinary disk can be written as

$$\frac{\tau_{\rm vis}^{\rm cbd}}{P_{\rm orb}} \sim 7.31 \times 10^5 \left(\frac{0.1}{\alpha_{\rm SS}}\right) \left(\frac{10^4\ {\rm K}}{T}\right) \left(\frac{M_{\rm BH}}{10^8\ M_\odot}\right) \left(\frac{0.01\ {\rm pc}}{a}\right), \quad (1)$$

where $\alpha_{\rm SS} = 0.1$ is the Shakura & Sunyaev (1973) viscosity parameter, $M_{\rm BH}$ is the total black hole mass, and a is the semi-major axis, respectively. The inner edge of the circumbinary disk is assumed to be at the $1:3$ resonance ($\sim 2.08\,a$), where the viscous force is balanced with the tidal/resonant force of the binary (Artymowicz & Lubow 1994). The circumbinary disk is assumed to follow an isothermal equation of state.

The mass transfer rate significantly depends on the binary orbital phase in eccentric binaries, whereas it shows little variation with orbital phase in circular binaries. In both cases the supermassive BBH system is expected to have triple disks because the mass transfer from the circumbinary disk would inevitably lead to the formation of an accretion disk around each black hole. However, there is little known about how the accretion disks are formed and what signatures they exhibit. We have, therefore, performed a new set of simulations at higher resolution, adopting the same set of binary orbital parameters we had previously used except for a semi-mjor axis $a = 0.01\,{\rm pc}$, which was chosen to yield a shorter period

binary than that of the previous simulation ($a = 0.1\,\mathrm{pc}$; Hayasaki et al. 2007).

The simulations should ideally take into account all of the processes at work in a triple-disk system, including mass transfer from the circumbinary disk to the individual black holes, and the accretion flow onto each black hole. Such a simulation, however, would require an enormous amount of computational time. Therefore, we divide these processes into a two-stage simulation. In the first stage, we investigate how the mass is transferred from the circumbinary disk to the effective gravitational radius of each black hole. In the second stage, we confine ourselves to simulate only the accretion onto each black hole by setting the mass-transfer rate from the first-stage simulation as a new boundary condition. In this paper, we focus on the results of the second-stage simulation.

2. Numerical Procedures

We set the binary orbit on the $x-y$ plane with the semi-major axis along the x-axis. Initially, each black hole is at the periastron. It orbits with $P_{\mathrm{orb}} \approx 9.4\,\mathrm{yr}$, and the orbital eccentricity is chosen to be $e = 0.5$. As a result of the interaction between the black holes and the neighboring stars and gas (Mayer et al. 2007), the BBH likely forms rapidly on scales of a few parsecs. The total black hole mass is $10^8 M_\odot$, which is a typical value for the centers of massive elliptical galaxies. The simulations were carried out with a total of 152,000 particles at the end, each one having a mass of $1.0 \times 10^{-15}\,M_{\mathrm{BH}}$. For simplicity, we set the mass ratio to $q \equiv M_2/M_1 = 1.0$ and assume that the circumbinary disk is coplanar with the binary orbital plane. The effect of the mass ratio, the orbital eccentricity, and inclination angle on the mass transfer process will be studied in a subsequent paper. In this section, we first explain the boundary conditions given by the first-stage simulation, followed by a brief description of the energy equation.

2.1. Boundary Conditions

To reduce computational time and to significantly improve the resolution, we confine the simulations only to the accretion flows around the supermassive BBH by supplying mass periodically from the outer boundary conditions, which are defined by the SPH particles captured by the black holes (Hayasaki & Okazaki 2004; Hayasaki et al. 2007). The capture radii correspond to the effective gravitational radii $0.8\,r_{\mathrm{L}}$, where r_{L} is the innermost common gravitational radius of the binary potential for a circular binary. The mass is added at a rate of $1\ M_\odot\,\mathrm{yr}^{-1}$ on the outer edge of the circumbinary disk. The system reaches quasi-steady

state equilibrium by 30 binary orbits, when the mass input balances the mass output. The mass of the circumbinary disk is $\sim 10^{-6}\,M_{\rm BH}$, and there are 56,870 SPH particles at the end of the simulation. To reduce the fluctuation noise, the data are folded over the orbital period $30 \le t \le 60$, where the unit of time, unless otherwise noted, is $P_{\rm orb} \simeq 9.4\,{\rm yr}$. The orbital phase dependence of the mass transfer rate obtained by this procedure is shown by the solid line in Figure 1. We model the mass transfer process from the circumbinary disk to the supermassive BBH by injecting gas particles at a given phase-dependent rate with spatial and velocity Gaussian distributions derived from the averaged values over $30 \le t \le 60$.

2.2. Energy Equation

The new simulations no longer assume an isothermal equation of state. We introduce an energy equation in order to resolve the temperature profile. The specific internal energy of an ideal gas is explicitly given by

$$u = \frac{K}{\gamma - 1}\rho^{\gamma-1}, \tag{2}$$

where ρ is the density, γ is the adiabatic index for an ideal gas (5/3), and K is a function of the entropy, which is obtained by the first law of thermodynamics. Time differentiation of equation (2) yields the energy equation, which can be written as

$$\frac{du}{dt} = \frac{P}{\rho^2}\frac{d\rho}{dt} + \frac{\rho^{\gamma-1}}{\gamma-1}\frac{dK}{dt}. \tag{3}$$

The first term on the right-hand side gives the heating of the gas at pressure P. In the current simulation, we assume that the heating due to viscosity is dissipated by cooling due to blackbody radiation. The cooling term is related to the effective temperature T by the Stefan-Boltzmann law,

$$\frac{2\sigma T^4}{\rho H_{\rm c}} = \frac{\rho^{\gamma-1}}{\gamma-1}\frac{dK}{dt}, \tag{4}$$

where σ is the Stefan-Boltzmann constant and $H_{\rm c}$ is the characteristic scale of the system, and the factor 2 represents radiation from the two sides of the accretion disk.

In SPH calculations, gas heating is implemented using a standard SPH artificial viscosity (Monaghan & Gingold 1983)

$$\Pi_{ij} = \begin{cases} (-\alpha_{\rm SPH} c_{\rm s}\mu_{ij} + \beta_{\rm SPH}\mu_{ij}^2)/\rho_{ij} & \text{for } \boldsymbol{v}_{ij}\cdot\boldsymbol{r}_{ij} \le 0 \\ 0 & \text{for } \boldsymbol{v}_{ij}\cdot\boldsymbol{r}_{ij} > 0 \end{cases} \tag{5}$$

for particle i and its neighboring particle j, where $\alpha_{\rm SPH}$ and $\beta_{\rm SPH}$ are the linear and nonlinear artificial viscosity parameters, respectively, $\rho_{ij} = (\rho_i + \rho_j)/2$ is the mean density, $\boldsymbol{r}_{ij} = \boldsymbol{r}_i - \boldsymbol{r}_j$

is the relative position vector, $\boldsymbol{v}_{ij} = \boldsymbol{v}_i - \boldsymbol{v}_j$ is the relative velocity vector, and $\mu_{ij} = h_{ij}\boldsymbol{v}_{ij} \cdot \boldsymbol{r}_{ij}/(r_{ij} + \eta_{ij})$ with $\eta_{ij}^2 = 0.01h_{ij}^2$ and $h_{ij} = (h_i + h_j)/2$ being the mean smoothing length. The entropy change of particle i can be written as (Bate 1995)

$$\frac{dK_i}{dt} = \frac{\gamma - 1}{2\rho_i^{\gamma-1}} \sum_j^{N_{\rm n}} m_j \Pi_{ij} \boldsymbol{v}_{ij} \cdot \boldsymbol{\nabla}_i W(\boldsymbol{r}_{ij}, h_{ij}), \tag{6}$$

where $N_{\rm n}$ is the number of neighboring particles and W, proportional to $|h_{ij}|^{-3}$, is called the SPH kernel. Thus, the effective temperature of particle i can be calculated from equations (4)-(6):

$$T_i = \left[\frac{\rho_i}{4\sigma} \sum_j^{N_{\rm n}} m_j h_{ij} \Pi_{ij} \boldsymbol{v}_{ij} \cdot \boldsymbol{\nabla}_i W(\boldsymbol{r}_{ij}, h_{ij}) \right]^{1/4}, \tag{7}$$

where we set $H_c = h_{ij}$ in the current simulation.

3. Accretion Disks around the Black Holes

Each of the two black holes has an accretion radius $5 \times 10^{-3}a$, which is the radius of the inner boundary of the simulation and corresponds to $r_{\rm in} \simeq 10.4\, r_{\rm BH}$, where $r_{\rm BH}$ is the Schwarzschild radius of a black hole with mass $5.0 \times 10^7\ M_\odot$. To verify the robustness of our simulation results, we have compared the averaged mass accretion rate during one orbital period with that of a simulation whereby the number of injected particles was doubled and the particle mass was reduced in half. We find no qualitative or quantitative differences to within $\sim 8\%$.

3.1. Formation Process

We use the standard SPH artificial viscosity throughout the simulations. In simulating the disks, the shear component of the SPH artificial viscosity can be replaced with the Shakura-Sunyaev viscosity parameter $\alpha_{\rm SS}$ in the following form: $\alpha_{\rm SS} = 0.1\alpha_{\rm SPH}h/H$ (Hayasaki et al. 2007), where h is the azimuthally averaged smoothing length and H is the azimuthally averaged scale height of the disk. The estimated value of $\alpha_{\rm SS}$ ranges from 0.001 to 0.2 over the entire region of the disk. Little gas can accrete viscously onto the black holes within the simulation run time because the viscous timescale is much longer than the orbital period (cf. Eq. 8).

The injected particles originally have eccentric orbits around the black holes because their angular momenta are smaller than that of the particles at the disk outer edge ($0.2\, a$).

Such gas particles accrete directly onto the black holes within one dynamical timescale of the disk, $\tau_{\rm dyn} = 2\pi/\Omega_{\rm disk} \sim 0.1 P_{\rm orb}$, which is estimated at the disk outer edge. In addition, the particles in each disk lose angular momentum mainly from tidal interaction with the other black hole because the timescale for angular momentum loss at the outer edge of the disk is shorter than the binary orbital period: $\tau_{\rm tide} \sim 2\pi/(\Omega_{\rm disk} - \Omega_{\rm orb}) \sim 0.1 P_{\rm orb}$, where $\Omega_{\rm disk}$ and $\Omega_{\rm orb}$ are the angular frequency of the disk and of the binary, respectively. This also makes it possible for the gas to accrete onto the black holes within the timescale of the binary orbit.

We illustrate the behavior of the two accretion disks in Figure 2, which gives snapshots of the accretion flow around the supermassive BBH covering one entire orbital period during the 10th binary orbit. At the end of the simulation, the disk has a mass of $\sim 10^{-8}\, M_{\rm BH}$. The two white crosses on each density map indicate the mass supply points. When the two black holes are closest together ($t = 10.0$), the disks are deformed due to the tidal interaction, and the supplied gas is added at the outer parts of the disks ($t = 10.04$). At $t = 10.1$, the gas particles that are added at the disk outer edge start to inspiral onto the black holes within a dynamical time. The disk size become $\sim 50\%$ smaller than the disk outer edge. As the black holes recede toward apastron ($t = 10.18$), the disks are restored from their tidal deformation and gradually circularize; tidal tails connect to the mass supply points between the two black holes. As can be seen in Figure 3*a*, during this time the temperature of the inner part of the disk is highest. The disks are connected to each other via tidal tails and are still eccentric, even at apastron ($t = 10.5$). The disks approach each other again toward the next periastron, and the injected particles once again start to be added to the disks ($t = 10.75$). This pattern repeats periodically.

3.2. Survival

Whether the accretion disks formed around the black holes are transient or persistent depends on the viscous timescale of the disk compared with the orbital period. For simplicity, we assume the accretion disk to be geometrically thin and isothermal with a Shakura-Sunyaev viscosity parameter $\alpha_{\rm SS}$. The ratio of the viscous timescale of a disk of size $R_{\rm d}$ to the orbital period is then given by

$$\frac{\tau_{\rm vis}^{\rm bhdisk}}{P_{\rm orb}} \sim 5.1 \times 10^5 \frac{1}{\sqrt{1+q}} \left(\frac{R_{\rm d}}{a}\right)^{1/2} \left(\frac{0.1}{\alpha_{\rm SS}}\right) \left(\frac{10^4 K}{T}\right) \left(\frac{0.01\,{\rm pc}}{a}\right) \left(\frac{M_{\rm BH}}{10^8 M_\odot}\right). \qquad (8)$$

It is immediately seen that the viscous timescale is much longer than the binary period. Thus, the accretion disks will survive, not only over the whole orbital phase but also over the simulation run-time ($\sim 10\, P_{\rm orb}$) once they are formed.

If the separation between the two black holes is less than 0.01 pc, emission of gravitational waves becomes the dominant mechanism to dissipate the binary's orbital energy (Begelman et al. 1980). Dissipation makes the binary evolve rapidly toward the coalescence of the two black holes. Therefore, we should consider whether the accretion disks survive with shrinkage of the semi-major axis due to gravitational wave emission. The merging timescale between two black holes due to the emission of gravitational radiation is given by (Peters 1964)

$$\frac{\tau_{\rm gr}}{P_{\rm orb}} \sim 6\times 10^5 \frac{(1+q)^2}{q} f(e) \left(\frac{0.01{\rm pc}}{a}\right)^{-5/2} \left(\frac{M_{\rm BH}}{10^8 M_\odot}\right)^{-5/2}, \tag{9}$$

where $f(e) = (1-e^2)^{7/2}/(1+73e^2/24+37e^4/96)$. From equations (7) and (8), we can compare the viscous timescale of the disk with the merging timescale:

$$\frac{\tau_{\rm vis}^{\rm bhdisk}}{\tau_{\rm gr}} \sim \frac{q}{(1+q)^{5/2}} \frac{1}{f(e)} \left(\frac{R_{\rm d}}{a}\right)^{1/2} \left(\frac{0.1}{\alpha_{\rm SS}}\right) \left(\frac{10^4 K}{T}\right) \left(\frac{0.01\,{\rm pc}}{a}\right)^{7/2} \left(\frac{M_{\rm BH}}{10^8 M_\odot}\right)^{7/2}. \tag{10}$$

The range of our simulation parameters satisfy $\tau_{\rm gr} \geq \tau_{\rm vis}^{\rm bhdisk} \gg P_{\rm orb}$. This ensures that the accretion disks, once formed, would survive until the black holes coalescence if the mass supply from the circumbinary disk to the central binary can be maintained. Gravitational wave emission has little influence on the formation and evolution of the accretion disks.

3.3. Temperature Profiles, Spectral Energy Distributions and Light Curves

The radial distribution of the azimuthally averaged temperature is shown in Figure 3*a*. The solid and dotted lines denote, respectively, the highest and lowest temperatures at $r_{\rm in}$. The gas is distributed over the entire region of the disk, and the temperature profile varies with orbital phase. Figure 3*b* shows the corresponding spectral energy distributions (SEDs) normalized by the Eddington luminosity for a total black hole mass $M_{\rm BH} = 1.0\times 10^8\ M_\odot$. The SEDs are computed numerically by integrating the spectrum, which is a function of disk temperature, from the outer edge of the disk ($0.2\,a$) to $r_{\rm in}$. Each SED has a peak in the ultraviolet (UV) region.

Figure 4*a* shows the orbital phase dependence of the light curves emitted from the disk in the UV, optical, and near-infrared (NIR) bands, obtained by averaging out the time variations over the orbital periods $10 \leq t \leq 11$. While the UV light curve shows substantial fluctuations with time, the optical and NIR light curves exhibit little variation. This is because a small temperature change produces large-amplitude variations in the UV region, where the SED decays exponentially (Fig. 3*b*), whereas it has little effect on the Rayleigh-Jeans part of the spectrum (optical and NIR). What does the X-ray light curve look like?

The dashed line in Figure 1 shows the orbital variation of the mass accretion rate, which is defined as the number of SPH particles per unit time captured at $r_{\rm in}$ over the orbital period $10 \leq t \leq 11$. If the gas in the disk accretes onto the black hole while keeping this orbital phase dependence, the X-ray light variation is expected to track the variation in mass accretion rate. This situation seems possible, if the accretion timescale in the inner region is shorter than the binary orbital period (i.e., close to the free-fall timescale), as is the case for radiatively inefficient accretion flows (Kato et al. 1998). The recent hydrodynamical simulations of supermassive BBHs by Bogdanović et al. (2008) predict strong X-ray outbursts during periastron passage. However, since our simulations do not take into account the relativistic correction of the gravitational potential in our simulations, the detail properties of the X-ray emission are beyond the scope of this work.

In order to isolate the effect of the mass transfer from the circumbinary disk onto the accretion disks, we carried out a simulation in which the mass transfer was artificially stopped over the orbital period $11 \leq t \leq 12$. For comparison purpose, the light curves for this case are shown in Figure 4*b*. Note that none of the light curves varies much with orbital phase. Thus, the periodic mass transfer from the circumbinary disk is clearly responsible for the significant variation of the UV light curve.

4. Summary and Discussion

We have performed SPH simulations of accretion flows around each black hole in a supermassive BBH system, taking into account periodic mass transfer from the circumbinary disk. An accretion disk forms and survives around each black hole. Thus, supermassive BBHs have triple disks, consisting of two accretion disks, one around each black hole, and a circumbinary disk surrounding them as a mass reservoir. In such systems, three dynamical processes are expected to give rise to structures in the two accretion disks. First, periodic mass transfer makes the disks eccentric because the gas particles from the circumbinary disk originally have elliptical orbits around the black holes. This makes it possible to accrete directly onto the black holes during the binary orbit. Second, once the disks form, periodic mass transfer from the circumbinary disk episodically gives an impact to the outer edge of the disks, resulting in the excitation of a one-armed spiral wave in the disks (e.g., Hayasaki & Okazaki 2005). Mass exchange between the two disks further reinforces the one-armed spiral wave. Finally, the disks are tidally deformed by the time-varying binary potential owing to the orbital eccentricity.

During the simulation, the accretion disks are still developing because their viscous timescale is much longer than the simulation run time ($10\,P_{\rm orb}$). In addition, a one-armed

spiral wave could also contribute to the non-axisymmetric disk structure because its propagation timescale, $\tau_{\rm wave} \sim (\alpha_{\rm SS}/2\pi)\tau_{\rm vis}^{\rm bhdisk} \sim 10^3 P_{\rm orb}$, is also much longer than the simulation run time (Hayasaki & Okazaki 2005). In such an early stage of the disk evolution, the periodic mass transfer has the dominant effect on the disk structure. Without mass transfer, tidal deformation alone has little influence on the light curve variation. As a consequence of the periodic mass transfer, we show that the light curve in the UV — and mostly likely also in the X-rays — exhibits variations with orbital phase, whereas little fluctuation is seen in the optical and NIR light curves. NIR variability might be detectable if the binary is surrounded by a dusty torus, whose inner edge would be irradiated by, and thus mirror, the variable central UV and X-ray sources. The photometric variability discussed in this paper is distinctive from the intrinsic variability normally seen from single accretion disks or jets, and thus provides a unique signature to identify BBH systems in galactic nuclei.

The orbital period of the fiducial case simulated here, ~ 9.4 yr, is long for any realistic observational experiment. The only known BBH candidate with a similar orbital period (11–12 yr) is the blazar OJ 287 (Sillanpää et al. 1988). Supermassive BBHs with shorter orbital periods (e.g., up to a few years) would be more practical observationally. However, the generic features of the triple-disk BBH system we have simulated would remain unchanged for shorter orbital periods. To avoid general relativistic corrections to the potential, the size of the accretion disk needs to be larger than $\sim 30\, r_{\rm BH}$. Since the semi-major axis of an equal-mass binary is $\gtrsim 20$ times the disk size, the results of our simulations can be scaled to systems with $a \gtrsim 600\ r_{\rm BH}$. This condition gives a wide range of tractable orbital periods, from $P_{\rm orb} = 5\,{\rm d}$ for $M_{\rm BH} = 10^6\, M_\odot$ to $P_{\rm orb} = 1.4\,{\rm yr}$ for $M_{\rm BH} = 10^8\, M_\odot$.

In the first-stage simulation, the orbital-phase dependence of mass transfer rate is smoothed out as the orbital eccentricity gets toward zero. On the other hand, the peak of the mass transfer rate in a higher eccentricity binary is sharper (cf. Hayasaki et al. 2007). These features can also be seen in the mass accretion rates and the light curves in the second-stage simulation. Most of the angular momentum gained from the mass transfer from the circumbinary disk is converted into that of the BBH via the tidal interaction between the BBH and the accretion disk. These processes damp the orbital eccentricity of the binary. However, since the damping timescale approximately equals the viscous timescale, which is much longer than the binary orbital period (cf. equation 8), this effect cannot be seen in this simulation.

When the separation between two black holes falls below $\sim 0.01\,{\rm pc}$, the binary will suffer rapid evolution due to the emission of gravitational radiation (Begelman et al. 1980). With the shrinkage of the semi-major axis, the gap between the circumbinary disk and the binary would be reformed. The timescale for gap reformation can be estimated as $\tau_{\rm gap} \sim 10^{-4}\tau_{\rm vis}^{\rm cbd}$

using equation (1) (cf. Artymowicz & Lubow 1994). If $\tau_{\rm gr} < \tau_{\rm gap}$, mass transfer from the circumbinary disk will be stopped, and the light curves from the system would exhibit little periodicity as in Figure 4*b*. On the other hand, if $\tau_{\rm gr} > \tau_{\rm gap}$, mass will continue to be supplied from the circumbinary disk to each black hole, and the BBH system will maintain triple disks. In this case, the periodic light curves predicted for the accretion disks can serve as the electromagnetic counterparts to gravitational wave events detectable with instruments such as *Laser Interferometer Space Antenna*.

We thank an anonymous referee for many useful comments and suggestions. K.H. is grateful to Atsuo T. Okazaki, Daisuke Kawata, and Hiroshi Sudou for helpful discussions. The authors thank YITP in Kyoto University, where this work was extensively discussed during the workshops YITP-W-05-11 on September 20–21, 2005 and YITP-W-06-20 on February 13–15, 2007. The simulations reported here were performed using the facility at the Centre for Astrophysics & Supercomputing at Swinburne University of Technology, Australia and at YITP in Kyoto University. This work was supported in part by the Grants-in-Aid of the Ministry of Education, Science, Culture, and Sport and Technology (MEXT; 30374218 K.H., 14079205 K.H. & S.M.), and by the Grant-in-Aid for the 21st Century COE Scientific Research Programs on "Topological Science and Technology" and "Center for Diversity and Universality in Physics" from MEXT.

REFERENCES

Armitage, P.J., & Natarajan, P. 2002, ApJ, 567, L9

——. 2005, ApJ, 634, 921

Artymowicz, P., & Lubow, S. H. 1994, ApJ, 421, 651

Bate, M. R. 1995, PhD thesis, Univ. Cambridge

Bate, M. R., Bonnel, I. A., & Price, N. M. 1995, MNRAS, 277, 362

Begelman, M. C., Blandford, R. D., & Rees, M. J. 1980, Nature, 287, 307

Benz, W. 1990, in Numerical Modeling of Nonlinear Stellar Pulsations: Problems and Prospects, ed. R. J. Buchler (Dordrecht: Kluwer), 269

Benz, W., Bowers, R. L., Cameron, A. G. W., & Press, W. H. 1990, ApJ, 348, 647

Bogdanović, T., Smith, B. D., Sigurdsson, S., & Eracleous, M. 2008, ApJ, submitted (arXiv:0708.0414)

Di Matteo, T., Springel, V., & Hernquist, L. 2005, Nature, 433, 604

Ebisuzaki, T., Makino, J., & Okumura, S.K. 1991, Nature, 354, 6350

Ferrarese, L., & Merritt, D. 2000, ApJ, 539, L9

Gebhardt, K., et al. 2000, ApJ, 539, L13

Gould, A., & Rix, H.-H. 2000, ApJ, 532, L29

Hayasaki, K., Mineshige, S., & Sudou, H. 2007, PASJ, 59, 427

Hayasaki, K., & Okazaki, A. T. 2004, MNRAS, 350, 971

——. 2005, MNRAS, 360, L15

Ivanov, P. B., Papaloizou, J. C. B., & Polnarev, A. G. 1999, MNRAS, 307, 79

Kato, S., Fukue, J., & Mineshige, S. 1998, Black-Hole Accretion Disks (Kyoto: Kyoto Univ. Press)

Komossa, S., Burwitz, V., Hasinger, G., Predehl, P., Kaastra, J. S., & Ikebe, Y. 2003, ApJ, 582, L15

Lobanov, A. P., & Roland, J. 2005, A&A, 431, 831

Magorrian, J., et al. 1998, AJ, 115, 2285

Makino, J. 1997, ApJ, 478, 58

Mayer, L., Kazantzidis, S., Madau, P., Colpi, M., Quinn, T., & Wadsley, J. 2007, Science, 316, 1874

Merritt, D., & Ekers, R. D. 2002, Science, 297, 1310

Milosavljević, M., & Merritt, D. 2001, ApJ, 563, 34

Monaghan J. J., & Gingold, R. A. 1983, J. Comput. Phys., 52, 374

Peters, P. C. 1964, Physical Review, 136, 1224

Rodriguez, C., Taylor, G. B., Zavala, R. T., Peck, A. B., Pollack, L. K., & Romani, R. W. 2006, ApJ, 646, 49

Roos, N. 1981, A&A, 104, 218

Shakura, N. I., & Sunyaev, R. A. 1973, A&A, 24, 337

Sillanpää, A., Haarala, S., Valtonen, M., Sundelius, B., & Byrd, G. G. 1988, ApJ, 325, 628

Sudou, H., Iguchi, S., Muratai, Y., & Taniguchi, T. 2003, Science, 300, 1263

Sundelius, B., Wahde, M., Lehto, H. J., & Valtonen, M. J. 1997, ApJ, 484, 180

Yu, Q. 2001, A&A, 377, 17

——. 2002, MNRAS, 331, 935

Yu, Q., & Tremaine, S. 2002, MNRAS, 335, 965

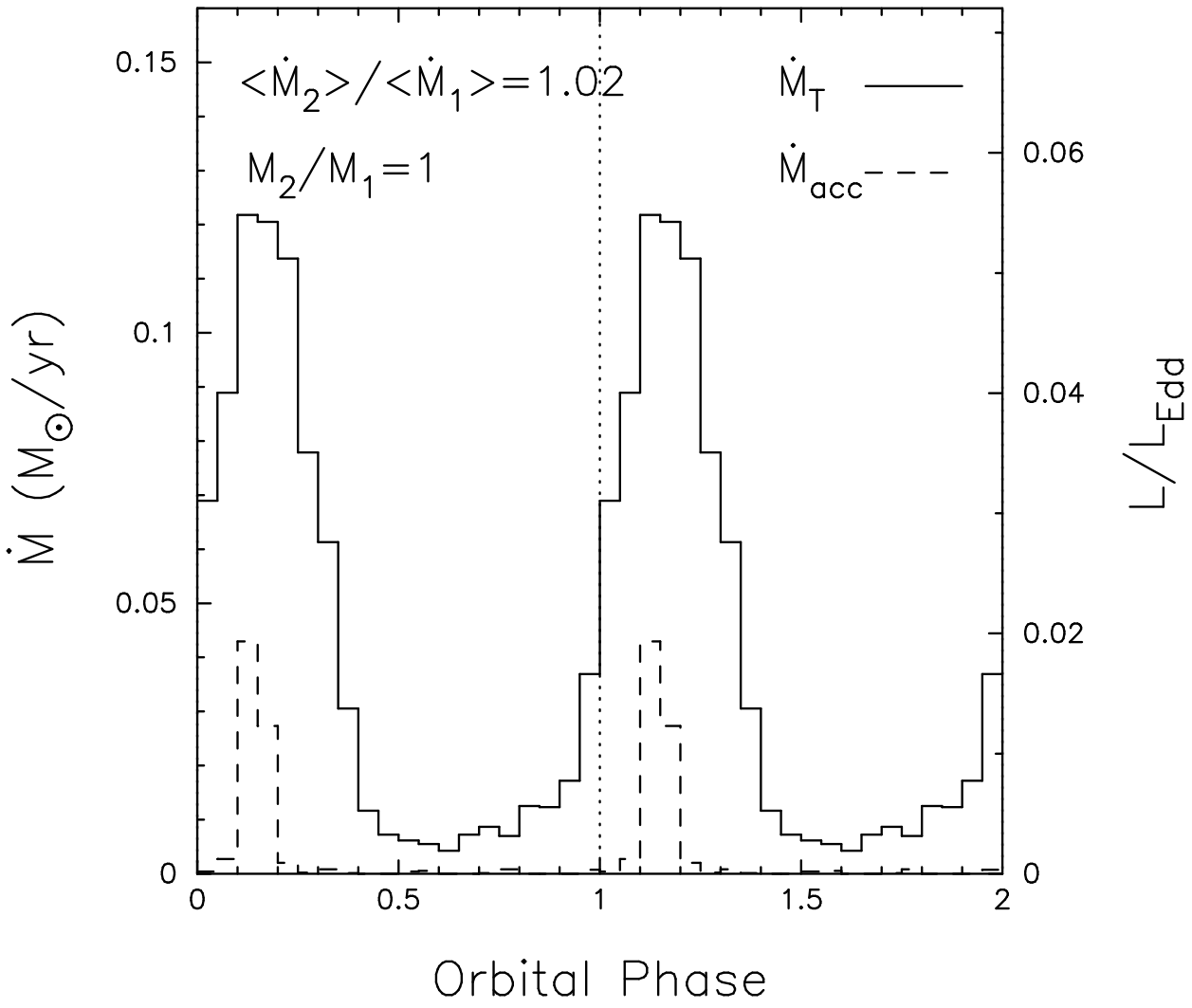

Fig. 1.— Orbital phase dependence of the mass transfer rate $\dot{M}_{\rm T}$ from the circumbinary disk to the effective common gravitational radius of the black holes, and of the mass accretion rate $\dot{M}_{\rm acc}$ at the inner simulation boundary, $r_{\rm in} = 5.0 \times 10^{-3} a$, of the primary black hole. The right axis shows the bolometric luminosity $L_{\rm bol}$ corresponding to the mass transfer and mass accretion rate with an energy conversion efficiency $\eta = 0.1$, normalized by the Eddington luminosity $L_{\rm Edd}$ for a total black hole mass $M_{\rm BH} = 1.0 \times 10^8\ M_\odot$, where η is defined by $L_{\rm bol} = \eta \dot{M}_{\rm BH} c^2$.

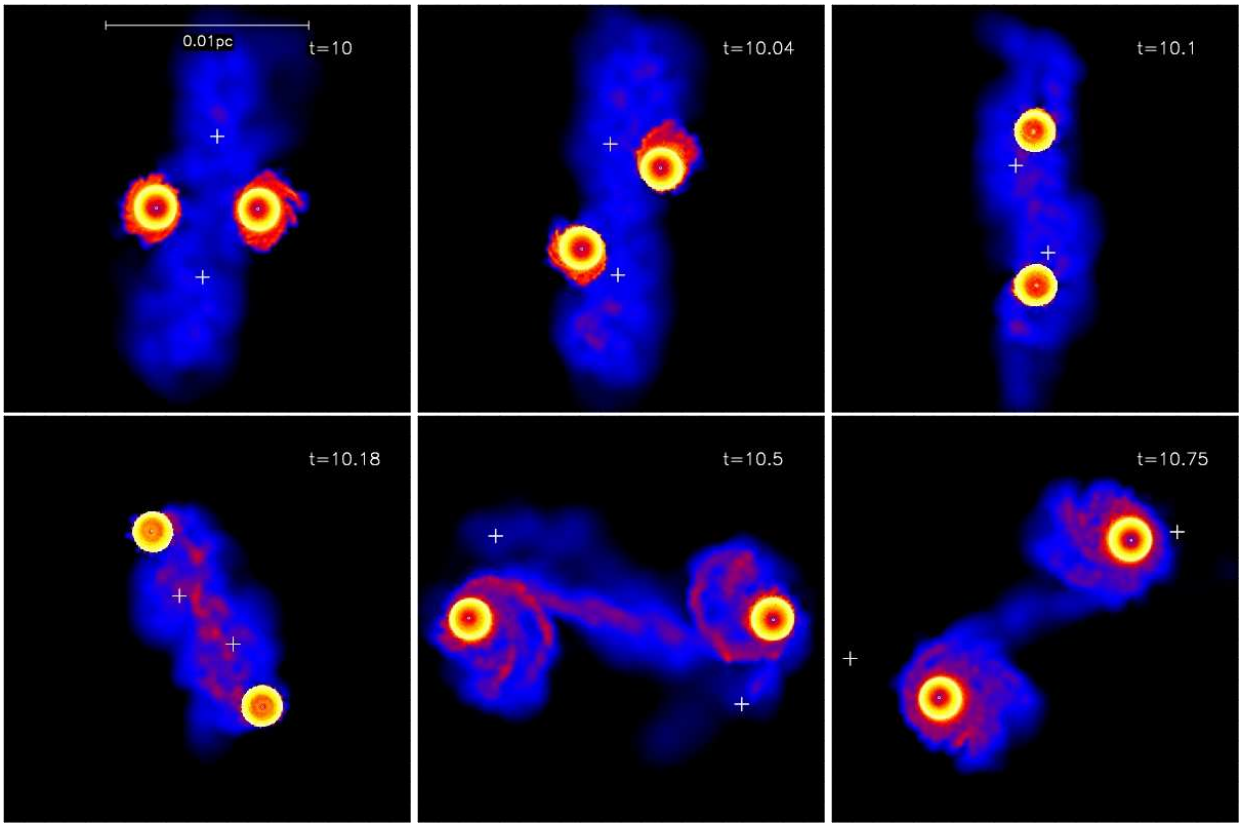

Fig. 2.— Density maps of the two accretion disks around the supermassive BBH rotating with $P_{\rm orb} \sim 9.4\,{\rm yr}$ and $e = 0.5$, for the period $10 \leq t \leq 11$. Each panel shows on a logarithmic scale the surface density contours over a range of 5 orders of magnitude. The white crosses indicate the positions of mass input (see text). The supermassive BBH is rotating in a counterclockwise direction. The time is shown in each panel, and a length scale is shown in the top-left panel. The number of SPH particles during this period ranges from $\sim 138,000$ to $152,000$.

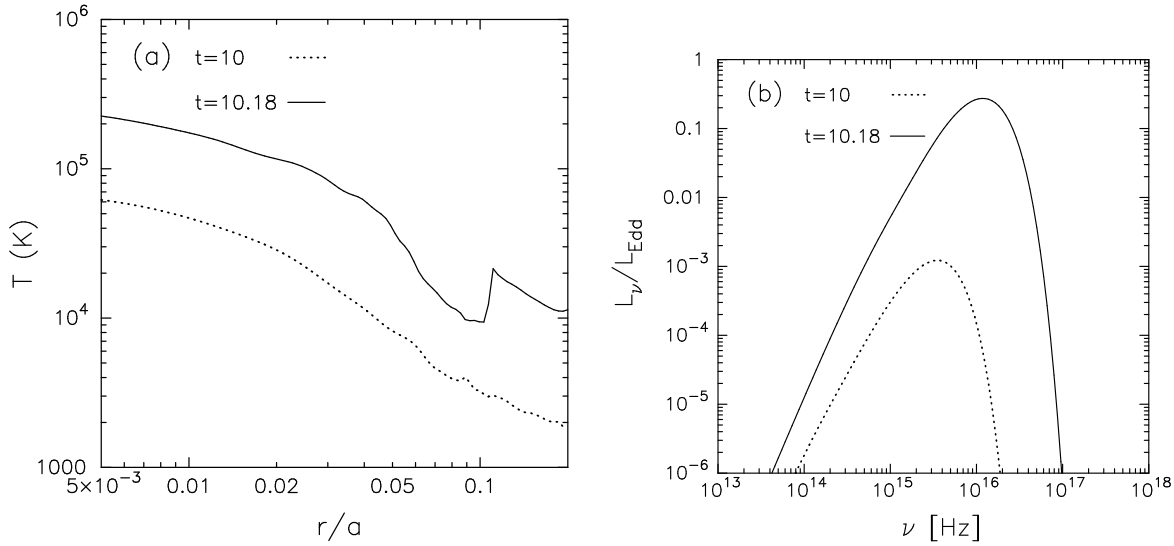

Fig. 3.— (a) Radial distribution of the azimuthally averaged disk temperature at $t = 10.0$ and at $t = 10.18$. (b) SEDs of the accretion disk around the black hole at $t = 10.00$ and $t = 10.18$. The integrated luminosity, $L_\nu = d^2\nu F_\nu$, is normalized by the Eddington luminosity $L_{\rm Edd}$ for a total black hole mass $M_{\rm BH} = 1.0 \times 10^8\ M_\odot$; F_ν is the flux at frequency ν and d is an arbitrary distance from the observer.

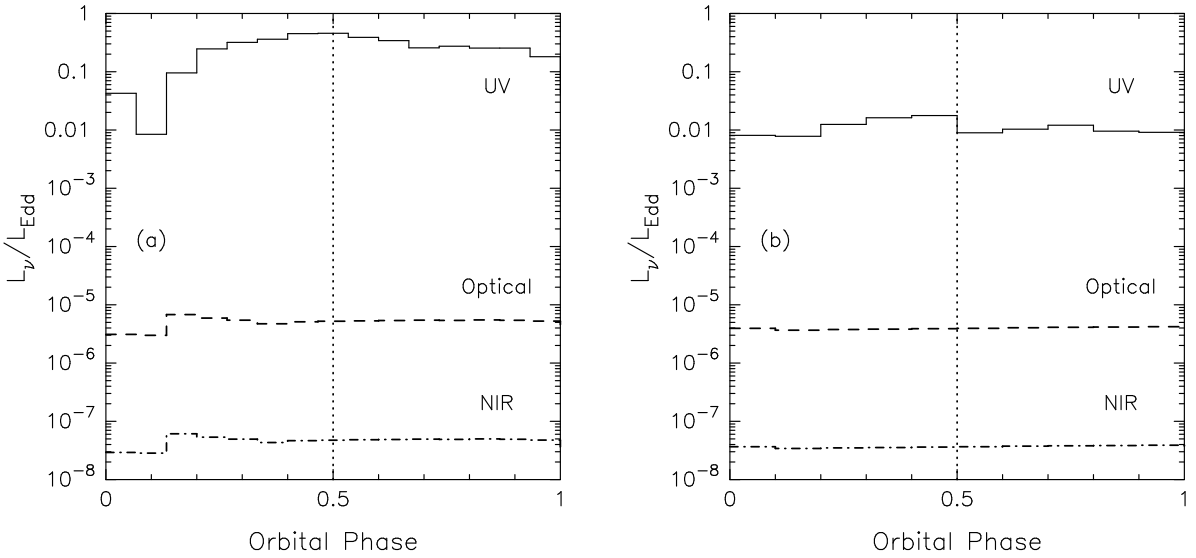

Fig. 4.— Orbital phase dependence of the UV ($\nu \simeq 1.0 \times 10^{16}$ Hz), optical (B band, $\nu \simeq 6.8 \times 10^{14}$ Hz), and NIR (K band, $\nu \simeq 1.36 \times 10^{13}$ Hz) light curves emitted from the disk. Panel (a) shows the light curves from the simulation with mass transfer, and panel (b) shows the light curves from the simulation with no mass transfer.

This figure "f2a.jpg" is available in "jpg" format from:

http://arXiv.org/ps/0708.2555v2

This figure "f2b.jpg" is available in "jpg" format from:

http://arXiv.org/ps/0708.2555v2

This figure "f2c.jpg" is available in "jpg" format from:

http://arXiv.org/ps/0708.2555v2

This figure "f2d.jpg" is available in "jpg" format from:

http://arXiv.org/ps/0708.2555v2

This figure "f2e.jpg" is available in "jpg" format from:

http://arXiv.org/ps/0708.2555v2

This figure "f2f.jpg" is available in "jpg" format from:

http://arXiv.org/ps/0708.2555v2